MorphSkein: A Shape-Changing Afterimage Display Preserving Pixel Density During Surface-Area Changes Across Troposkein-Based Shapes

MAXIME DANIEL, Univ. Bordeaux, ESTIA Institute of Technology, EstiaR, France
SHARIFF AM FALEEL, University of British Columbia, Okanagan, Canada
POURANG IRANI, University of British Columbia, Okanagan, Canada

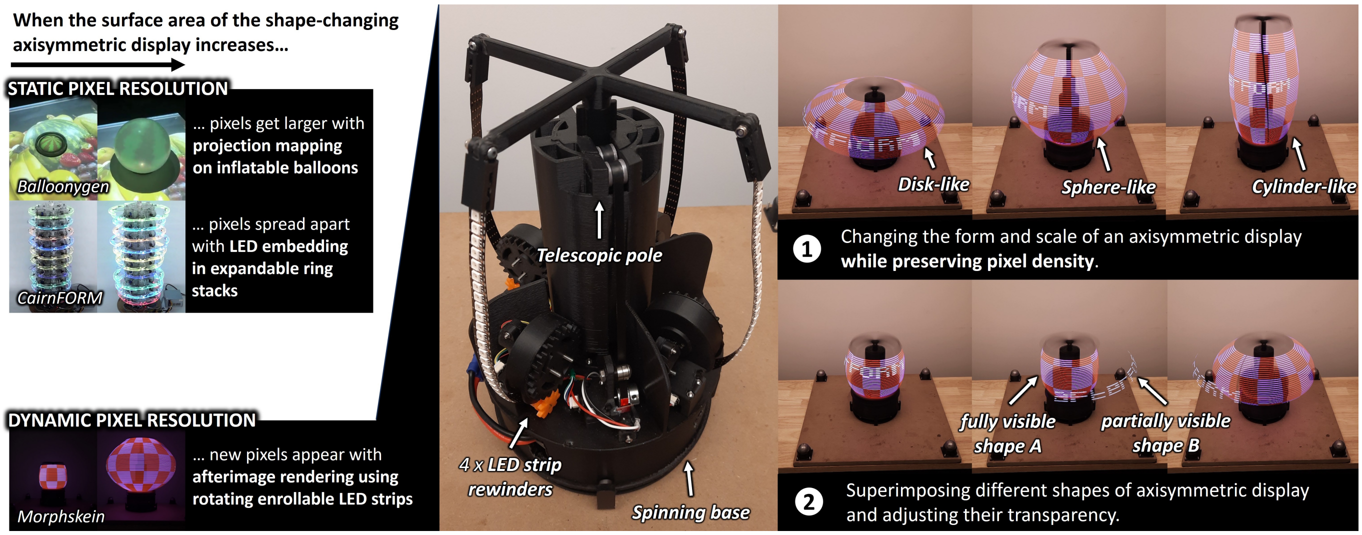

Fig. 1. Inspired by *troposkeins*[1], MorphSkein is an afterimage display performing axisymmetric (360°-visible) shape transformations while maintaining pixel density: it combines a spinning base, a telescopic pole, and LED strip rewinders to generate troposkein-based afterimages, dynamically adjusting pixel resolution to match the displayed surface. Our technique enables control over the form, scale, transparency, and superimposition of axisymmetric displays.

Shape-changing displays typically lose pixel density as surface area expands, limiting their usability. We introduce MorphSkein, a shape-changing afterimage display that preserves initial density (1.44 px/cm²) across naturally occurring axisymmetric shapes generated by spinning cables (troposkeins). The system uses a telescopic pole and four LED-strip rewinders on a rotating base. As the strips spin, centrifugal force forms troposkeins, and persistence of vision creates 360°-visible displays, while adjusting pole height and strip lengths changes their shape. As surface area grows, pixel density is preserved vertically by releasing new rows from the rewinders and horizontally by rendering extra columns per revolution with the strips. This keeps comparable density along the central horizontal line of the display, with naturally higher density toward the top and bottom where the troposkein curves inward. Because the technique relies on a mathematical model assuming ideal troposkein geometry, angular velocity becomes critical: incorrect speeds degrade pixel density accuracy, axisymmetric shape fidelity, or both. Interpolation of experimental data shows that 69.44% of reachable troposkein configurations achieve ⩾90% density accuracy and shape fidelity for at least one operating speed. Remaining cases degrade due to insufficient motor speed or limited MCU speed and LED refresh rate. Limitations and improvements are discussed.

CCS Concepts: • **Human-centered computing → Displays and imagers**.

ACM Reference Format:
Maxime Daniel, Shariff AM Faleel, and Pourang Irani. 2026. MorphSkein: A Shape-Changing Afterimage Display Preserving Pixel Density During Surface-Area Changes Across Troposkein-Based Shapes. *ACM Trans. Graph.* 45, 4, Article 40 (July 2026), 11 pages. https://doi.org/10.1145/3811320

1 Introduction

Axisymmetric shapes are symmetric around an axis and enable 360°-visible displays that communicate information to all surrounding users. Such displays appear in various forms (e.g., cone [3CINNODisplay 2024], sphere [Machida 2002], cylinder [Yendo et al. 2005]) at different scales (e.g., hand [Priyadarshana et al. 2016], desk [Miyafuji et al. 2017], room [Machida 2002]). However, fixed geometry limits their versatility across applications and scales. First, each form induces application-specific distortions, such as spherical mapping for planet textures [Machida 2002] or cylindrical mapping for avatar bodies [Bolton et al. 2012]. Second, small systems [Miyafuji et al. 2017; Priyadarshana et al. 2016] cannot present large-scale content, while large systems [Bolton et al. 2012; Machida 2002; Yendo et al.

Authors' Contact Information: Maxime Daniel, m.daniel@estia.fr, Univ. Bordeaux, ESTIA Institute of Technology, EstiaR, Bidart, France; Shariff AM Faleel, shariff.mohommedfaleel@ubc.ca, University of British Columbia, Okanagan, Kelowna, Canada; Pourang Irani, pourang.irani@ubc.ca, University of British Columbia, Okanagan, Kelowna, Canada.

This work is licensed under a Creative Commons Attribution 4.0 International License.
© 2026 Copyright held by the owner/author(s).
ACM 1557-7368/2026/7-ART40
https://doi.org/10.1145/3811320

2005] are too bulky for compact spaces despite supporting small images.

Shape-changing axisymmetric displays address these limitations, using approaches like projection mapping on inflatable balloons [Toyohara et al. 2018] or LEDs embedded in expandable ring stacks [Daniel and Rivière 2021; Daniel et al. 2019; Lakatods 2012], allowing dynamic adaptation to different forms and scales. However, existing shape-changing systems have *static pixel resolution* and cannot maintain density as their surface area grows—pixels enlarge like balloons or spread along expanding rings. This causes two main issues: first, enlarged or spaced pixels reduce clarity and sharpness, making text, charts, and images harder to read and increasing user effort and fatigue [Legge et al. 1985; Näsänen and Ojanpää 2003]. Second, without adding pixels, larger displays cannot show more content or higher resolution, limiting their usefulness compared to multiple static displays. Preserving pixel density during transformations is therefore essential for usability.

Inspired by *troposkeins*[1], we introduce MorphSkein—a shape-changing axisymmetric display that preserves pixel density across varying surface areas via *dynamic pixel resolution* (Figure 1, left). Unlike prior systems using LED embedding or projection mapping, our prototype leverages afterimage rendering to maintain density across naturally forming axisymmetric shapes traced by a spun cable (*troposkeins*). The system enables control over the form, scale, transparency, and superimposition of axisymmetric displays (Figure 1, right). It consists of a telescopic pole and four LED strip rewinders mounted on a spinning base (Figure 1, center). As the strips spin, centrifugal force forms troposkeins, and persistence of vision creates 360°-visible displays. Shape control uses two parameters: the telescopic pole adjusts the height of all troposkeins, while each rewinder sets individual lengths. A density of 1.44 px/cm is preserved vertically by releasing new 7 mm-pitch rows from the rewinders for longer troposkeins, while horizontally additional columns are rendered per revolution for wider troposkeins to maintain a 7 mm pitch along the central horizontal line. Away from this line, the troposkein curves inward toward the top and bottom, reducing horizontal pixel pitch below 7 mm and increasing density beyond 1.44 px/cm.

Because the technique relies on a mathematical model assuming ideal troposkein geometry, angular velocity becomes critical to maintain pixel density and shape fidelity. We describe the system and evaluate how angular speed affects these metrics. The system supports 16985 display configurations spanning troposkein lengths of 21.7–75.6 cm and heights of 20–50 cm (radii 13.4–44.4 cm). Interpolation from 18 measured configurations shows that 69.44% of all configurations achieve $\geqslant$90% accuracy on both metrics for at least one speed within 150–330 RPM (10–22 Hz refresh rate). These high-performance configurations are concentrated primarily within radii of 21–42.2 cm (68.39% of the range). At smaller radii, shape fidelity degrades due to insufficient motor speed, while at larger radii, pixel density degrades due to insufficient MCU speed and LED refresh rate. Finally, we discuss limitations (user safety and physical interaction, shape variety and stability) and opportunities for improvement (pixel density, frame rate, image size, color depth, pixel alignment, display aperture, and noise).

[1]A troposkein (derived from the Greek; literally, "turning rope") is the shape assumed by a flexible object such as a cable or rope resulting from centrifugal forces when the cable is swung about an axis through its ends.

2 Related Work

Shape-Changing Interfaces (SCIs) [Alexander et al. 2018; Ishii et al. 2012; Strohmeier et al. 2016] are interactive systems that physically transform in response to user inputs or system events, enabling new ways to convey information, reconfigure interfaces, and augment users. As users are accustomed to the high visual fidelity of modern displays, similar expectations extend to shape-changing displays [Alexander et al. 2018]. However, maintaining high pixel density during shape transformation remains challenging: expanding surfaces require additional pixels, and without preserving density, visual quality degrades at larger scales, reducing usability. In the following, we focus on literature related to preserving pixel density in shape-changing axisymmetric displays. Additionally, we discuss prior work on volumetric displays, to which MorphSkein contributes by enabling adjustable view-volume boundaries.

2.1 Using Afterimage Rendering For Preserving Pixel Density Amidst Axisymmetric Shape Transformations

Traditional axisymmetric displays primarily rely on embedded LEDs [Machida 2002; Priyadarshana et al. 2016] or projection mapping [Li et al. 2019; Miyafuji et al. 2017] to render 360-degree images on static axisymmetric shapes. These techniques also underpin shape-changing variants, including projection mapping on inflatable balloons [Toyohara et al. 2018], embedding LEDs in expandable ring stacks [Daniel and Rivière 2021; Daniel et al. 2019; Lakatods 2012]. However, these systems struggle to maintain pixel density during shape transformation because they have *static pixel resolution*: as the surface area increases, pixels enlarge on inflating balloons, while pixels spread apart as ring perimeters expand. Pixel density therefore decreases with increasing surface area. A third technique, afterimage rendering [Yamada et al. 2017; Yendo et al. 2005], is widely known for static axisymmetric displays but has not yet been explored in shape-changing contexts. Afterimage displays rapidly rotate LED arrays around an axis, sequentially emitting pixel columns that integrate perceptually through Persistence of Vision (PoV) [Di Lollo et al. 1988]. To appear continuous, each pixel column must be refreshed at least 16 times per second, following the flicker-fusion threshold [Davis 1955]. Unlike embedded LEDs or projection mapping, afterimage rendering inherently supports *dynamic horizontal pixel resolution*: the number of pixel columns displayed per revolution can vary. We leverage this capability to develop a shape-changing axisymmetric display that adapts its pixel resolution as its surface area changes.

2.2 Enabling Adjustable View-Volume Boundaries in Volumetric Displays

Volumetric displays dynamically fill a 3D space with voxels visible from any angle without special eyewear. Existing systems operate within fixed view-volume boundaries [Hirayama et al. 2019; Ochiai et al. 2016; Sullivan 2002; Wu et al. 2010; Yendo et al. 2010; Yoshida 2016]. MorphSkein can be regarded as volumetric display with adjustable view-volume boundaries. It belongs to the *rotationally swept*

Table 1. Comparison of the MorphSkein system with prior systems in terms of axisymmetric shape domain and degrees of freedom, as well as pixel refresh rate and density. (*) denotes values not explicitly reported in the original publications but estimated from available information. (≥) indicates a minimum pixel density, reflecting non-uniform distribution across the surface.

	Shape		**Pixel**	
System	**Domain**	**Degrees of freedom**	**Refresh**	**Density**
CairnFORM [Daniel et al. 2019]	cylinder → local cylindrical deformations	10 expandable rings (*local widths*, ∅35 → 62 cm)	400 Hz*	*h*: 0.21 → 0.12 px/cm (-43%)* *v*: 0.12 px/cm*
Balloonygen [Toyohara et al. 2018]	disk → global spherical deformations	1 inflatable balloon (*global width and height*, ∅10 → 30 cm*)	120 Hz*	*h*: 108 → ≥11.4 px/cm (-89%)* *v*: 108 → ≥11.4 px/cm (-89%)*
MorphSkein	cylinder → global layered troposkein deformations	4 strip rewinders (*global layer widths*, ∅26.4 → 88.8 cm) 1 telescopic pole (*global height*, 20 → 50 cm)	10–22 Hz	*h*: ≥1.44 → ≥1.44 px/cm *v*: 1.44 → 1.44 px/cm

volume systems category [Hahn et al. 2023], which typically rotate an LED panel to generate concentric cylinder-shaped layers of voxels within a fixed volume [Wu et al. 2010]. In contrast, MorphSkein rotates multiple flexible LED strips of varying lengths, forming concentric troposkein-shaped layers of voxels within a view volume with adjustable boundaries. The spacing between all layers can be modified by actuating the telescopic pole and LED strip rewinders. This enables the device to adjust its view-volume dimensions to suit different installation contexts and supports attention-grabbing applications (Figure 6).

3 MorphSkein System

MorphSkein is a system that facilitates axisymmetric shape-change without losing pixel density in the process. See Table 1 for comparison with prior work in terms of axisymmetric shape transformation and pixel density preservation capabilities. Our system comprises a telescopic pole and four LED strip rewinders mounted on a spinning base. As the LED strips spin around the pole, centrifugal force shapes them into troposkeins. This results in the user perceiving the surface of an axisymmetric display because of the persistence of vision. The system controls **three key parameters** (Figure 2):

v : the angular velocity (RPM) of all four troposkeins via the spinning base;

h : the height (mm) of all troposkeins via the telescopic pole;

$l = (l_1, l_2, l_3, l_4)$: the lengths (mm) of the four troposkeins, with each l_i independently set by its corresponding LED strip rewinder.

The frame rate f (FPS) of an axisymmetric display rendered by MorphSkein is

$$f = (v \times n)/60 \tag{1}$$

where n is the number of LED strips used to render the afterimage of the same display shape. Increasing the rotational speed v or the number of strips n raises the frame rate. For example, four strips at 150 RPM yield 10 FPS, while at 360 RPM they reach 24 FPS. Similarly, one strip at 360 RPM produces 6 FPS, while four strips reach 24 FPS.

3.1 Display Transformation Capabilities

The MorphSkein system enables a fourfold design space for shape-changing axisymmetric displays (Figure 1): **form change**, where adjusting strip lengths while fixing pole height alters the form; **scale change**, where proportional adjustments of pole height and strip lengths change the scale; **shape transparency**, achieved by selectively rendering pixels for partial or full transparency; and **shape superimposition**, where combining different strip lengths creates layered displays. See Figure 6 for example applications.

3.2 Hardware Implementation

Figure 7 provides a visual representation and detailed description of the key components comprising the MorphSkein system. The spinning base supports 330 angular speeds ($v \in \{1, 2, \ldots, 330\}$ RPM), the telescopic pole offers 301 pole heights ($h \in \{200, 201, 202, \ldots, 500\}$ mm), and each LED strip rewinder enables 78 strip lengths in 7mm increments ($l \in \{217, 224, 231, \ldots, 756\}$ mm). Combining h and l yields 16985 unique troposkeins, with $l - h > 14\,mm$ enforcing a two-LED offset to prevent strip damage from excessive bending.

3.3 Maintaining Pixel Density Throughout Axisymmetric Shape-Change

As the MorphSkein system undergoes axisymmetric shape-change, a vertical pixel density of 1.44 px/cm is maintained in hardware: as the display's vertical surface area increases, the rewinder extends the LED strip, releasing pixel rows at a fixed 7 mm pitch. The **vertical pixel resolution** (number of pixel rows) is therefore computed as:

$$p = 7 \quad \mathbf{res_v} = l/p \tag{2}$$

where p is the constant LED-strip pitch (mm) and res_v is the vertical pixel resolution.

In comparison, a minimum horizontal pixel density of 1.44 px/cm is enforced in software: as surface area increases, additional pixel columns (7 mm spacing along the central horizontal line) are rendered to match the display perimeter, with pixel density naturally increasing toward the top and bottom where the troposkein curves inward. The display perimeter is computed from the troposkein geometry (see Figure 2) as follows:

$$w_{offset} = 94.5 \quad r = w + w_{offset} \quad P = 2\pi r \tag{3}$$

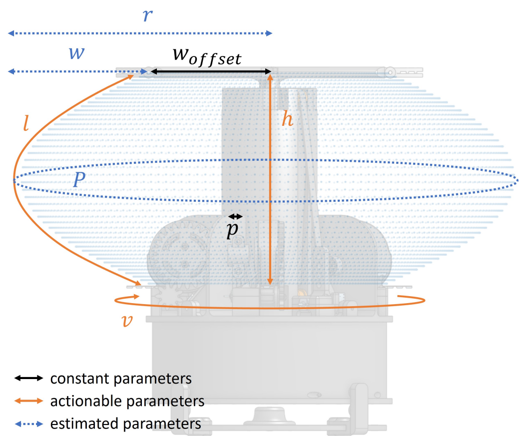

Fig. 2. MorphSkein system parameters: **Constant parameters** (black) include the 7 mm pixel pitch (p) and the 94.5 mm troposkein offset (w_{offset}) from the rotational axis. **Actionable parameters** (orange) include angular speed (v), pole height (h), and strip length (l). **Estimated parameters** (blue), derived from both constant and actionable values, include the troposkein width (w), display radius (r), and display perimeter (P).

where w_{offset} is the fixed troposkein offset from the rotational axis (mm), w is the troposkein width, and r and P are the radius and perimeter of the display (mm). The **horizontal pixel resolution** (number of pixel columns per revolution) required to maintain a minimum horizontal pitch of 7 mm is then:

$$\mathbf{res_h} = P/p \quad T = 6 \times 10^{10}/v \tag{4}$$

where res_h is the horizontal pixel resolution and T is the duration of a single revolution, expressed in time units (ns).

3.3.1 Troposkein Model. Equation 3 cannot be evaluated without first determining w, the width of the troposkein. To obtain this quantity, we use a mathematical model [Banks 2013] based on the complete elliptic integrals of the first and second kinds, $K(m)$ and $E(m)$, and the incomplete elliptic integral of the first kind, $F(\phi, m)$, where m is the elliptic-integral parameter and ϕ is the amplitude:

$$\begin{aligned} K(m) &= \int_0^{\pi/2} \left[1 - m\sin(t)^2\right]^{-1/2} dt \\ E(m) &= \int_0^{\pi/2} \left[1 - m\sin(t)^2\right]^{1/2} dt \\ F(\phi, m) &= \int_0^{\phi} \left[1 - m\sin(t)^2\right]^{-1/2} dt \end{aligned} \tag{5}$$

The 2D curve of a troposkein is described as

$$x = \frac{h}{2} \times \left[1 - \frac{F(\phi, m)}{K(m)}\right] \qquad y = w \times \sin\phi \tag{6}$$

and the troposkein width and the strip length are given as:

$$w = h \times \frac{m}{(1-m^2)K(m)} \qquad l = h \times \frac{2}{(1-m^2)}\frac{E(m)}{K(m)} - 1 \tag{7}$$

3.3.2 Numerical Estimation and Pixel Resolution Mapping. For each of the 16985 troposkeins reachable by our prototype (Section 3.2), we used a numerical solver to estimate the elliptic-integral parameter m for the target strip length l, given the pole height h. The solver defines a loss function that measures the absolute difference between the target strip length and the one predicted by Equation 7-right:

$$loss(m; h, l) = |l - (h \times \frac{2}{(1-m^2)}\frac{E(m)}{K(m)} - 1)| \tag{8}$$

Elliptic integrals are computed via Carlson's duplication algorithm [Carlson 1979] to a precision of 10^{-16}, and Brent's method [Brent 1973] is then used to minimize the loss over $m \in (0, 1)$ with a tolerance of 10^{-7}. The resulting parameter is substituted into Equation 7-left to compute the corresponding troposkein width. Using Equations 2 and 4, we then calculate the pixel resolution to construct the lookup table

$$R : (h_i,\ l_i) \mapsto (res_{h,i}, res_{v,i}) \mid i = 1, \ldots, 16985 \tag{9}$$

mapping each reachable $(h_i,\ l_i)$ pair to its corresponding pixel resolution $(res_{h,i},\ res_{v,i})$. The lookup table is then embedded in the ESP32 source code, saving computation time that can instead be used to render additional pixel columns per revolution.

3.3.3 Software Implementation. At time t, with a 2D RGB input image $I : (x, y) \mapsto (r, g, b)$, Algorithm 1 describes the infinite loop the ESP32 uses to render afterimages with one or more LED strips.

Algorithm 1 afterimage rendering using one or more LED strips

Require: t ▷ current time (ns)
T ▷ revolution duration (ns)
h ▷ pole height (mm)
$l = (l_1, \ldots, l_n)$ ▷ length of each active LED strip (mm)
$R : (h, l) \mapsto (res_h, res_v)$ ▷ pixel resolution lookup table
$I : (x, y) \mapsto (r, g, b)$ ▷ input 2D RGB image
$x' = (x'_1, \ldots, x'_n)$ ▷ last rendered column for each strip

while true **do**
  for $i = 1$ **to** $len(l)$ **do**
    $(res_h, res_v) \leftarrow R(h, l_i)$ ▷ Get display pixel resolution
    $inv_T \leftarrow t/T$ ▷ Compute normalized time (global phase)
    $inv_N \leftarrow i/len(l)$ ▷ Compute strip's relative phase offset
    $\phi \leftarrow (inv_T + inv_N) \bmod 1$ ▷ Compute phase in $[0, 1)$
    $x \leftarrow floor(\phi \times res_h)$ ▷ Get current image column
    if $x \neq x'_i$ **then**
      for $y = 1$ **to** res_v **do**
        set color of the y^{th} LED to $I(x, y)$
      end for
      $x'_i \leftarrow x$
    end if
  end for
end while

3.3.4 Model Limitations. Importantly, the model we employed describes the 2D curve of a troposkein and ignores the effects of the following factors on the LED strips: angular speed, gravity, third dimension, aerodynamic drag, tension, and material properties. Recent studies have introduced advanced models that analyze the 3D

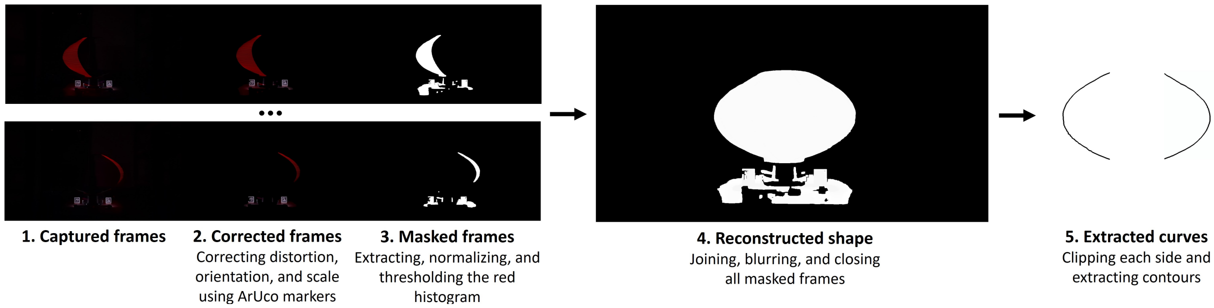

Fig. 3. Image processing sequence performed on individual LED strips for each trial.

curve of a troposkein while considering one or more of these factors [Aristoff and Stone 2012; Yong 2006]. However, these models are designed for regular ropes and do not apply to flexible LED strips (i.e., irregular ropes made of various materials with different rigidity and density).

4 Technical Evaluation

Angular speed is crucial for the MorphSkein system as it generates the centrifugal force required to shape the LED strip into a troposkein, following Newton's laws. However, our mathematical model cannot compute the required angular speed based on pole height and strip length (see *3.3.4 Model Limitations*). This creates challenges for two key aspects of **Axisymmetric Shape Fidelity**:

- **Axisymmetric Shape Accuracy**: Insufficient angular speed produces too little centrifugal force to form the expected troposkein, resulting in irregular curvature (bumps along the strip remain unsmoothed) and an axisymmetric, mushroomhead-like shape (gravity pulls the strip downward).
- **Axisymmetric Shape Stability**: Insufficient angular speed also prevents all LED strips from forming the same troposkein. Variations in curvature between strips can produce a visual wobble when multiple strips contribute to the same display (each strip render the same pixel at slightly different 3D positions).

Angular speed also impacts two components of **Pixel Density Accuracy**:

- **Pixel Pitch Accuracy**: Insufficient angular speed causes the display perimeter to be overestimated, yielding a pixel pitch along the central horizontal line of the display below 7 mm (gravity pulls the LED strip down, reducing the actual troposkein width compared to the computed value).
- **Pixel Resolution Integrity**: Excessive angular speed can prevent all pixel columns from being rendered within a single revolution, leading to skipped columns and a reduction in horizontal pixel resolution (fewer pixel columns per revolution than expected due to hardware speed limitations).

We conducted a technical evaluation to assess the impact of angular speed on the pixel density and the shape fidelity of the MorphSkein system.

4.1 Factors

We considered the following target values for the key parameters during the technical evaluation:

- $v_{test} \in \{150, 180, 210, 240, 270, 300, 330\}$ *RPM*: Seven different angular speeds corresponding to a framerate from 10 Hz to 22 Hz in 2 Hz steps for a display generated using all four LED strips.
- $h_{test} \in \{200, 300, 400, 500\}$ *mm*: Four different pole heights representing a scale factor from 1 to 2.5 in 0.5 steps.
- $l_{test} \in \{217, 322, 434, 539, 651, 756\}$ *mm*: Six different strip lengths representing a scale factor from 1 to 3.5 in 0.5 steps.

Valid (h_{test}, l_{test}) pairs with $l_{test} > h_{test}$ yield eighteen distinct display radii (r_{test}).

4.2 Measurements

For each (h_{test}, l_{test}) pair, we computed:

- *Expected curve*: Solved Equation 6 to estimate the 2D troposkein curve.
- *Expected horizontal pixel pitch*: Set at 7 mm for all troposkeins along the central horizontal line of the display.
- *Expected horizontal pixel resolution*: Solved Equation 7 to estimate troposkein width, then determined pixel columns per revolution using Equations 3 and 4.

For each v_{test} condition of each (h_{test}, l_{test}) pair, we recorded a video with one LED strip illuminated in red. From the video, we derived:

- *Observed curve*: Extracted the 2D troposkein curve via image processing (see Figure 3).
- *Observed horizontal pixel pitch*: Estimated along the central horizontal line of the display using the observed curve width and solving Equations 3 and 4.
- *Observed horizontal pixel resolution*: Logged using Algorithm 1 (line 8), if $x - x'_i = 1$ no columns are skipped; if $x - x'_i > 1$ then $x - x'_i - 1$ columns are skipped between consecutive renders.

4.3 Variables

Using the previous measurements, we computed the following response variables for each strip in each trial:

- **Axisymmetric Shape Accuracy**: Percentage of *observed curve* area matching the *expected curve* area. We compute the area under each curve up to the vertical reference line at w_{offset} using the algorithm described in [Jekel et al. 2019]. The matching percentage is defined as $1 - \frac{A_{diff}}{max(A_{obs}, A_{exp})}$ where A_{diff} is the area between the observed and expected curves of a strip, and A_{obs} and A_{exp} are the areas under the observed and expected curves of the strip, respectively, computed up to w_{offset}.

- **Axisymmetric Shape Stability**: Percentage of *observed curve* area shared among all four LED strips, computed pairwise. The matching percentage between strips i and j is defined as $1 - \frac{A_{diff,i,j}}{max(A_{obs,i}, A_{obs,j})}$ where $A_{diff,i,j}$ denotes the area between the observed curves of strips i and j, and $A_{obs,i}$ and $A_{obs,j}$ are the areas under the observed curves of strips i and j, respectively, computed up to the vertical reference line at w_{offset}.
- **Pixel Pitch Accuracy**: Percentage of *observed horizontal pixel pitch* over the *expected horizontal pixel pitch.*
- **Pixel Resolution Integrity**: Percentage of *observed horizontal pixel resolution* over the *expected horizontal pixel resolution.*

4.4 Apparatus and Procedure

Figure 4 shows the setup for the MorphSkein system's technical evaluation. A Samsung Galaxy A51 was placed 30 cm above the ground, 250 cm from the system's center, in a dark room. ArUco markers were attached to each side of the system, illuminated by a spotlight for visibility, aiding image processing to correct frame scale and orientation. For each (h_{test}, l_{test}) pair, the following steps were performed: **(1) Reset** – the system stops the spinning base, retracts the pole to 200 mm and pulls all strips to 217 mm. **(2) Initialization** – the system spins the base to 150 RPM, pushes all strips to l_{test} and extends the pole to h_{test}. **(3) Trials** – for each v_{test}, the system adjusts the base speed and turns off all strips. One by one, each strip is lit in red for 1 second, followed by 500 milliseconds off.

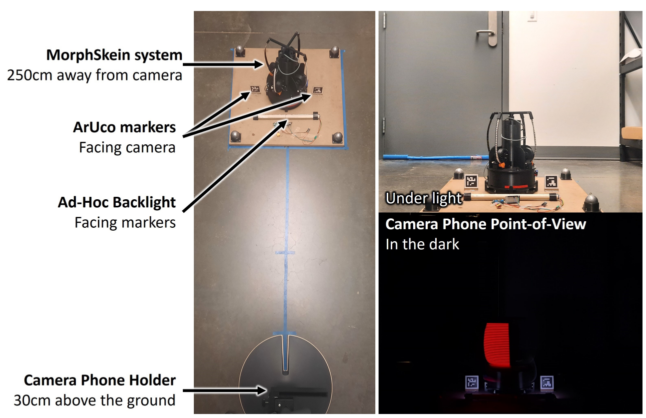

Fig. 4. Apparatus for the technical evaluation of the MorphSkein system.

4.5 Results

Figure 8-top shows the aggregate mean of each variable with respect to angular speed and display radius, along with the corresponding pole height and strip length. Figure 8-right presents the linear regressions and Pearson correlations for each variable. Because pole height must exceed strip length, the height and length datasets have uneven sample sizes (e.g., a 217 mm strip was tested with a 200 mm pole but not with pole heights of 300–500 mm). To obtain matched samples, trials below 539 mm strip length were excluded from both datasets (pairwise trimming). The following paragraphs analyze the effect of each factor on each variable.

4.5.1 *Pixel Resolution Integrity.*

Values range from 38% to 100%, with a mean of 79.5% ± 20.2% (95% CI [0.783, 0.808]). As anticipated, integrity decreases as the base spins faster [r(1008)=-.58, p<.001] or as the display gets wider [r(1008)=-.73, p<.001] (as the strip gets longer [r(672)=-.47, p<.001]). Nevertheless, as shown in Figure 8, the system preserves 100% integrity for at least one RPM setting at every display radius between 134 mm and 365 mm—covering 82% of the tested radius range. The system fails to maintain integrity once angular speed and radius require rendering a pixel column every 7 mm under 1.214 ± 0.008 ms, exceeding the limits of a single 240 MHz ESP32 MCU sequentially driving four 32 MHz LED strips (Figure 7). Notably, integrity improves with increasing pole height [r(672)=.36, p<.001] because the same strip length and angular speed ranges were used at all heights: taller poles yield narrower troposkeins, increasing the time available to render each pixel column within the hardware's constraints.

4.5.2 *Pixel Pitch Accuracy.*

Values span from 82.5% to 100%, averaging at 94.5% ± 3.4% (95% CI [0.943, 0.947]). In contrast to pixel resolution integrity, pixel pitch accuracy increases as the base spins faster [r(1008)=.20, p<.001] or as the display radius widens [r(1008)=.75, p<.001] (i.e., as the strip lengthens [r(672)=.37, p<.001]). As the strip moves faster around the center or away from the center, it experiences increased centrifugal force. This results in the observed troposkein width approaching the expected value, leading the MorphSkein system to render a pixel pitch closer to 7 mm. Notably, we observe a decrease in pixel pitch accuracy as the pole height increases [r(672)=-.38, p<.001]. Again, our experimental setup maintains the same strip length range and angular speed range for each pole height: the LED strips ultimately get closer to the center and thus experience less centrifugal force as the pole height increases, leading the observed strip width further away from the expected troposkein width.

4.5.3 *Axisymmetric Shape Accuracy.*

Values range from 43.6% to 98.3%, with a mean of 85.6% ± 11.1% (95% CI [0.849, 0.863]). Similar to pixel pitch accuracy, shape accuracy improves as the base spins faster [r(1006)=.23, p<.001] or as the display gets wider [r(1008)=.75, p<.001] (i.e., as the strip gets longer [r(672)=.42, p<.001]). Indeed, the strip experiences increased centrifugal force as it moves faster around the center or away from the center. As a result, the observed strip curve elevates and converges toward the expected troposkein curve. For the same reason as for pixel pitch accuracy, we observe that shape accuracy decreases as the pole height increases [r(672)=-.34, p<.001].

4.5.4 *Axisymmetric Shape Stability.*

Values span from 63.3% to 99.7%, averaging at 95.2% ± 5.5% (95% CI [0.949, 0.954]). Stability increases with display radius [r(1386)=.48, p<.001] and strip length [r(1386)=.20, p<.001], as greater distance from the center increases centrifugal force and drives all strip curves toward the same expected troposkein, improving multi-strip coherence. In contrast, stability decreases with pole height [r(882)=-.59, p<.001]. Two factors likely explain this strong negative correlation: (1) with fixed strip length and angular speed ranges, taller poles position the strips closer to the center, reducing centrifugal force and increasing deviations from the expected troposkein; and (2) greater pole height introduces mechanical play in the telescopic assembly, causing slight pole tilt and vertical asymmetry among the four strips, which reduces visual stability when multiple strips are used.

4.6 Aggregation

Figure 8 shows the overall performance of the MorphSkein system in terms of *pixel density accuracy* and *axisymmetric shape fidelity*. These high-level scores are computed as the arithmetic means of, respectively, pixel resolution integrity with pixel pitch accuracy, and axisymmetric shape accuracy with axisymmetric shape stability.

4.6.1 Pixel Density Accuracy. Scores range from 66.1% to 99.6%, averaging at 87% ± 9.1% (95% CI [0.865, 0.876]). In the top right corner, pixel density dips below 95% accuracy as the axisymmetric display widens and accelerates, correlating with the results on pixel resolution integrity. Conversely, in the bottom left corner, pixel density also falls below 95% accuracy as the axisymmetric display narrows and decelerates, correlating with the results on pixel pitch accuracy. Within this range, a noticeable valley emerges, where the MorphSkein system maintains pixel density above 95% accuracy, highlighting an optimal balance between pixel resolution integrity and pixel pitch accuracy.

4.6.2 Axisymmetric Shape Fidelity. Scores span from 66.7% to 98.1%, averaging at 90.5% ± 6.9% (95% CI [0.901, 0.909]). Correlating with the results on shape accuracy and shape stability, shape fidelity increases as the axisymmetric display widens and speeds up. Three distinct zones stand out: (1) for radius ranging from 134 mm to 294 mm, shape fidelity is below 90% accuracy; (2) between 210 mm and 294 mm, shape fidelity fluctuates between 90% and 95% accuracy; and (3) for radii spanning from 327 mm to 444 mm, shape fidelity surpasses 95% accuracy. Notably, shape fidelity deteriorates at radii 181, 282, and 351 mm when the telescopic pole is fully extended to 500 mm, due to lateral tilting in this fully extended state.

4.7 Interpolation

Based on the experimental data (Figure 8) obtained for 18 sampled configurations $(h_{test}, l_{test}, r_{test})$ across 7 speeds (v_{test}), we used linear radial basis function interpolation to estimate performance across all 16985 configurations (h, l, r) across those speeds. Figure 5 presents the resulting estimates. Applying a 90% threshold yields:

- *Pixel Density Accuracy*: 16924 (99.64%) configurations (display radii ≈134–422 mm) meet the threshold for at least one tested angular speed between 150–330 RPM.
- *Axisymmetric Shape Fidelity*: 13590 (80.01%) configurations (radii ≈210–444 mm) meet the threshold for at least one tested speed.
- *Combined Performance*: 11795 (69.44%) configurations (radii ≈210–422 mm) satisfy both thresholds for at least one speed.

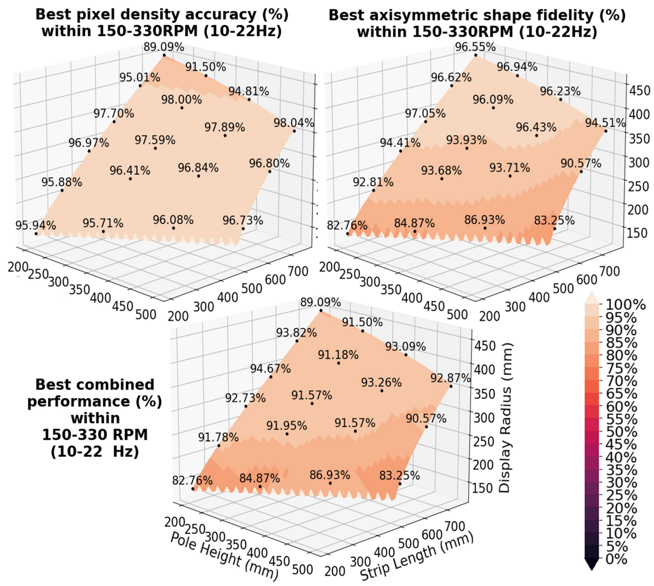

Fig. 5. Estimated best performance within 150–330 RPM (10–22 Hz) across 16985 configurations, interpolated from the measured samples: (**left**) pixel density accuracy, (**right**) axisymmetric shape fidelity, and (**bottom**) combined performance (min of both). (•) denotes the 18 tested configurations with measured values.

5 Conceptual Limitations

5.1 User Safety and Physical Interaction

Shape-changing interfaces typically support direct physical interaction through dynamic surfaces [Alexander et al. 2018], which is unsafe with MorphSkein due to its high-speed rotating LED strips. While some rotating displays enable safe touch interaction [Yang et al. 2026], we prioritize pixel density preservation and axisymmetric shape transformation. Alternative modalities such as gestures [Tahouni et al. 2020], proxemics [Ballendat et al. 2010], and speech [Taher et al. 2015] remain viable. Safety risks can be further mitigated by mounting the system above human height indoors [Schardt et al. 2015] or on a drone outdoors [Yamada et al. 2017].

5.2 Shape Variety and Stability

MorphSkein is limited to troposkein-based shapes, and achieving uniform shaping across multiple LED strips is challenging, leading to slight afterimage jitter. Vibrations from the extending telescopic pole worsen this, though industrial manufacturing techniques can help. As a replacement for flexible LED strips, LED-embedded motorized chains with closed-loop curvature control [Nakagaki et al. 2016, 2015] could enable uniform shaping and axisymmetric forms beyond troposkeins while reducing or eliminating jitter. However, these motorized chains must remain lightweight and robust to endure high angular speeds.

5.3 Volumetric Display Limitations

As a volumetric display, MorphSkein provides adjustable view-volume boundaries but has limitations. First, it generates directional voxels that are visible when facing the LED strips, rather than from all directions. Second, voxel distribution is constrained by concentric troposkein layers, producing non-uniform voxel density that increases toward the top and bottom. Finally, voxel density is not preserved in all three dimensions during view-volume expansion. Although intra-layer density is maintained as layer surface area increases, the spacing between layers also increases. With no additional layers (i.e., LED strips) introduced, overall voxel density decreases along the depth dimension. Future work could address these limitations by exploring shape-changing volumetric displays that preserve constant and uniform voxel density across all three dimensions during volume expansion, maintaining usability.

6 Technical Improvements

6.1 Pixel Density and Frame Rate

MorphSkein preserves a minimum pixel density of 1.44 px/cm² and a maximum refresh rate of 22 FPS at 330 RPM with four LED strips rendering the same display. Both metrics can be improved through hardware upgrades without altering the core concept. Horizontal density can be increased by rendering more columns per revolution using a faster MCU, higher-refresh LED strips, or one dedicated MCU per strip instead of driving all strips sequentially with a single MCU and two multiplexers (Figure 7). Vertical density can be improved by switching to smaller-pitch strips, or doubled by placing two strips side by side, each offset by half a pitch. Frame rate can be increased by raising the maximum angular speed using a more powerful motor, provided the MCU and LED strips can support the higher speed. Alternatively, it can be improved by using more LED strips to render the same display, achieved by integrating additional strip rewinders.

6.2 Image Size and Color Depth

Due to the ESP32's limited on-chip memory (520 KB SRAM, with approximately 50 KB available after firmware upload), the MorphSkein system can store only two 250×100 px images at 8-bit color depth. This limitation imposes three key constraints: only two displays can be rendered simultaneously; each display is capped at a 360° surface of 1.225 m²; and the system cannot exploit the full range of human color perception at 8-bit depth. Potential solutions include adding external memory (up to 4 MB PSRAM), adopting a MCU with greater on-chip memory, such as the Teensy (1 MB SRAM), or distributing computation by assigning a dedicated MCU to each LED strip.

6.3 Pixel Shape and Alignment

The LED strips in MorphSkein produce rectangular pixels by continuously rendering columns without gaps, resulting in horizontally stretched afterimages. Disabling the strip after each column would yield square pixels but double activations per revolution; we avoid this to maximize horizontal resolution, though faster-refresh strips could mitigate the trade-off. Furthermore, maintaining the strips within the rotation plane is essential for the vertical alignment of pixel columns. While flexible ropes (e.g., nylon strings) can curl out of plane under aerodynamic forces [Aristoff and Stone 2012], LED strips exhibit limited widthwise flexibility, reducing such deflection. However, some vertical misalignment may still occur, causing vertically curled afterimages. A technical evaluation could quantify aerodynamic effects on alignment and enable correction by correlating misalignment with pole height, strip length, and angular speed.

6.4 Display Aperture and Noise Level

Positioning the LED strip ends parallel to the telescopic pole creates a permanent aperture at the top of the display (Figure 1). To eliminate this, the ends of all LED strips can be consolidated into a single point atop the pole. However, this requires modifying the troposkein model to account for non-parallel LED strip ends. Additionally, friction in the brushed motor and between metal bearings and the 3D-printed spinner generates noise around 80 dB at 330 RPM. Switching to a brushless motor and using materials like aluminum for the spinner can reduce noise and increase the maximum achievable angular speed.

7 Conclusion

Existing shape-changing axisymmetric displays use static resolution, causing pixel density to decrease as surface area increases and limiting usability. We introduce MorphSkein, which maintains a baseline density of 1.44 px/cm² across troposkein-based shapes via dynamic resolution. Density naturally increases beyond this baseline toward the top and bottom, where the troposkein curves inward. Because this technique assumes ideal troposkein geometry, angular velocity is critical for both density accuracy and shape fidelity. The system supports 16985 display configurations spanning troposkein lengths of 21.7–75.6 cm and heights of 20–50 cm (radii 13.4-44.4 cm). Based on 18 measured configurations and interpolation over all configurations, 69.44% achieve ⩾90% density accuracy and shape fidelity for at least one speed between 150–330 RPM, mainly within a 21–42.2 cm radius range (68.39% of the range). Performance is limited by motor speed at smaller radii and by MCU speed and LED refresh rate at larger radii. Finally, we discuss limitations including safety, shape variety, and stability, and outline improvements to image size, color depth, pixel density, frame rate, pixel alignment, noise, and the top aperture.

References

3CINNODisplay. 2024. Cone Shape Creative Screen in Resort Theme Park. Available at https://www.led-display-manufacturer.com/cases/business/cone-shape-screen-in-resort-theme-park/ (Accessed: 2025-03-20).

Jason Alexander, Anne Roudaut, Jürgen Steimle, Kasper Hornbæk, Miguel Bruns Alonso, Sean Follmer, and Timothy Merritt. 2018. Grand Challenges in Shape-Changing Interface Research. In *Proceedings of the 2018 CHI Conference on Human Factors in Computing Systems (CHI '18)*. Association for Computing Machinery, Montreal QC, Canada, 1–14. doi:10.1145/3173574.3173873

Jeffrey M. Aristoff and Howard A. Stone. 2012. The aerodynamics of jumping rope. *Proceedings of the Royal Society A: Mathematical, Physical and Engineering Sciences* 468, 2139 (March 2012), 720–730. doi:10.1098/rspa.2011.0389

Till Ballendat, Nicolai Marquardt, and Saul Greenberg. 2010. Proxemic interaction: designing for a proximity and orientation-aware environment. In *ACM International Conference on Interactive Tabletops and Surfaces* (Saarbrücken, Germany) *(ITS '10)*. Association for Computing Machinery, New York, NY, USA, 121–130. doi:10.1145/1936652.1936676

Robert B. Banks. 2013. *Towing icebergs, falling dominoes, and other adventures in applied mathematics.* Princeton University Press, Princeton, NJ.

John Bolton, Peng Wang, Kibum Kim, and Roel Vertegaal. 2012. BodiPod: Interacting with 3d Human Anatomy via a 360° Cylindrical Display. In *CHI '12 Extended Abstracts on Human Factors in Computing Systems (CHI EA '12)*. Association for Computing Machinery, New York, NY, USA, 1039–1042. doi:10.1145/2212776.2212380 event-place: Austin, Texas, USA.
Richard P. Brent. 1973. *Algorithms for Minimization without Derivatives* (1st ed.). Prentice-Hall, Englewood Cliffs, New Jersey.
B. C. Carlson. 1979. Computing elliptic integrals by duplication. *Numer. Math.* 33, 1 (March 1979), 1–16. doi:10.1007/BF01396491
Maxime Daniel and Guillaume Rivière. 2021. Exploring Axisymmetric Shape-Change's Purposes and Allure for Ambient Display: 16 Potential Use Cases and a Two-Month Preliminary Study on Daily Notifications. In *Proceedings of the Fifteenth International Conference on Tangible, Embedded, and Embodied Interaction*. ACM, Salzburg Austria, 1–6. doi:10.1145/3430524.3442452
Maxime Daniel, Guillaume Rivière, and Nadine Couture. 2019. CairnFORM: a Shape-Changing Ring Chart Notifying Renewable Energy Availability in Peripheral Locations. In *Proceedings of the Thirteenth International Conference on Tangible, Embedded, and Embodied Interaction - TEI '19*. ACM Press, Tempe, Arizona, USA, 275–286. doi:10.1145/3294109.3295634
S. W. Davis. 1955. Auditory and Visual Flicker-Fusion as Measures of Fatigue. *The American Journal of Psychology* 68, 4 (Dec. 1955), 654. doi:10.2307/1418795
Vincent Di Lollo, Craig D. Clark, and John H. Hogben. 1988. Separating visible persistence from retinal afterimages. *Perception & Psychophysics* 44, 4 (July 1988), 363–368. doi:10.3758/BF03210418
Joonku Hahn, Woonchan Moon, Hosung Jeon, Minwoo Jung, Seongju Lee, Gunhee Lee, and Muhan Choi. 2023. Volumetric 3D Display: Features and Classification. *Current Optics and Photonics* 7, 6 (Dec. 2023), 597–607. doi:10.3807/COPP.2023.7.6.597
Ryuji Hirayama, Diego Martinez Plasencia, Nobuyuki Masuda, and Sriram Subramanian. 2019. A volumetric display for visual, tactile and audio presentation using acoustic trapping. *Nature* 575, 7782 (Nov. 2019), 320–323. doi:10.1038/s41586-019-1739-5
Hiroshi Ishii, Dávid Lakatos, Leonardo Bonanni, and Jean-Baptiste Labrune. 2012. Radical Atoms: Beyond Tangible Bits, Toward Transformable Materials. *interactions* 19, 1 (Jan. 2012), 38–51. doi:10.1145/2065327.2065337
Charles F. Jekel, Gerhard Venter, Martin P. Venter, Nielen Stander, and Raphael T. Haftka. 2019. Similarity measures for identifying material parameters from hysteresis loops using inverse analysis. *International Journal of Material Forming* 12, 3 (01 May 2019), 355–378. doi:10.1007/s12289-018-1421-8
David Lakatods. 2012. *AMPHORM: Form Giving through Gestural Interaction to Shape Changing Objects*. Master's thesis. Massachusetts Institute of Technology, Cambridge, MA, USA.
Gordon E. Legge, Denis G. Pelli, Gar S. Rubin, and Mary M. Schleske. 1985. Psychophysics of reading—I. Normal vision. *Vision Research* 25, 2 (1985), 239–252. doi:10.1016/0042-6989(85)90117-8
Zhengqing Li, Shio Miyafuji, Erwin Wu, Hideaki Kuzuoka, Naomi Yamashita, and Hideki Koike. 2019. OmniGlobe: An Interactive I/O System For Symmetric 360-Degree Video Communication. In *Proceedings of the 2019 on Designing Interactive Systems Conference*. ACM, San Diego CA USA, 1427–1438. doi:10.1145/3322276.3322314
Tamotsu Machida. 2002. GEO-COSMOS: World's First Spherical Display. In *ACM SIGGRAPH 2002 Conference Abstracts and Applications (SIGGRAPH '02)*. Association for Computing Machinery, New York, NY, USA, 189. doi:10.1145/1242073.1242202 event-place: San Antonio, Texas.
Shio Miyafuji, Toshiki Sato, Zhengqing Li, and Hideki Koike. 2017. Qoom: An Interactive Omnidirectional Ball Display. In *Proceedings of the 30th Annual ACM Symposium on User Interface Software and Technology*. ACM, Québec City QC Canada, 599–609. doi:10.1145/3126594.3126607
Ken Nakagaki, Artem Dementyev, Sean Follmer, Joseph A. Paradiso, and Hiroshi Ishii. 2016. ChainFORM: A Linear Integrated Modular Hardware System for Shape Changing Interfaces. In *Proceedings of the 29th Annual Symposium on User Interface Software and Technology - UIST '16*. ACM Press, Tokyo, Japan, 87–96. doi:10.1145/2984511.2984587
Ken Nakagaki, Sean Follmer, and Hiroshi Ishii. 2015. LineFORM: Actuated Curve Interfaces for Display, Interaction, and Constraint. In *Proceedings of the 28th Annual ACM Symposium on User Interface Software & Technology*. ACM, Charlotte NC USA, 333–339. doi:10.1145/2807442.2807452
Risto Näsänen and Helena Ojanpää. 2003. Effect of image contrast and sharpness on visual search for computer icons. *Displays* 24, 3 (2003), 137–144. doi:10.1016/j.displa.2003.09.003
Yoichi Ochiai, Kota Kumagai, Takayuki Hoshi, Jun Rekimoto, Satoshi Hasegawa, and Yoshio Hayasaki. 2016. Fairy Lights in Femtoseconds: Aerial and Volumetric Graphics Rendered by Focused Femtosecond Laser Combined with Computational Holographic Fields. *ACM Transactions on Graphics* 35, 2 (May 2016), 1–14. doi:10.1145/2850414
Lahiru Lakmal Priyadarshana, Victoria Porter, Juan Pablo Carrascal, Aaron Visser, and Roel Vertegaal. 2016. MagicWand: Exploring Physical Affordances with a Handheld Cylindrical Display Object. In *Proceedings of the 2016 CHI Conference Extended Abstracts on Human Factors in Computing Systems*. ACM, San Jose California USA, 3762–3765. doi:10.1145/2851581.2890259
Philipp Schardt, Michael Schmitz, Hannes Käfer, and Eric Hofmann. 2015. Lichtform: A Shape Changing Light Installation. In *Proceedings of the 4th International Symposium on Pervasive Displays*. ACM, Saarbruecken Germany, 259–260. doi:10.1145/2757710.2776811
Paul Strohmeier, Antonio Gomes, Giovanni Maria Troiano, Aske Mottelson, Timothy Merritt, and Jason Alexander. 2016. Sharing Perspectives on the Design of Shape-Changing Interfaces. In *Proceedings of the 2016 CHI Conference Extended Abstracts on Human Factors in Computing Systems*. ACM, San Jose California USA, 3492–3499. doi:10.1145/2851581.2856478
Alan Sullivan. 2002. LP-1: Late-News Poster: The DepthCube™ Solid-state Multi-planar Volumetric Display. *SID Symposium Digest of Technical Papers* 33, 1 (May 2002), 354–355. doi:10.1889/1.1832925
Faisal Taher, John Hardy, Abhijit Karnik, Christian Weichel, Yvonne Jansen, Kasper Hornbæk, and Jason Alexander. 2015. Exploring Interactions with Physically Dynamic Bar Charts. In *Proceedings of the 33rd Annual ACM Conference on Human Factors in Computing Systems (CHI '15)*. Association for Computing Machinery, New York, NY, USA, 3237–3246. doi:10.1145/2702123.2702604 event-place: Seoul, Republic of Korea.
Yasaman Tahouni, Isabel P. S. Qamar, and Stefanie Mueller. 2020. NURBSforms: A Modular Shape-Changing Interface for Prototyping Curved Surfaces. In *Proceedings of the Fourteenth International Conference on Tangible, Embedded, and Embodied Interaction*. ACM, Sydney NSW Australia, 403–409. doi:10.1145/3374920.3374927
Soichiro Toyohara, Toshiki Sato, and Hideki Koike. 2018. Balloonygen: extended tabletop display embedded with balloon-like deformable spherical screen. In *Proceedings of the 24th ACM Symposium on Virtual Reality Software and Technology*. ACM, Tokyo Japan, 1–5. doi:10.1145/3281505.3281532
Jiang Wu, Caijie Yan, Xinxing Xia, Jia Hou, Haifeng Li, Xu Liu, and Wenting Zheng. 2010. 44.2: An Analysis of Image Uniformity of Three-dimensional Image Based on Rotating LED Array Volumetric Display System. *SID Symposium Digest of Technical Papers* 41, 1 (May 2010), 657–660. doi:10.1889/1.3500551
Wataru Yamada, Kazuhiro Yamada, Hiroyuki Manabe, and Daizo Ikeda. 2017. iSphere: Self-Luminous Spherical Drone Display. In *Proceedings of the 30th Annual ACM Symposium on User Interface Software and Technology (UIST '17)*. ACM, New York, NY, USA, 635–643. doi:10.1145/3126594.3126631 event-place: Québec City, QC, Canada.
Willa Yunqi Yang, Justice T Andersen, David Dajun Yuan, and Ken Nakagaki. 2026. BloomBeacon: Blooming Physical Touch Display Surfaces via Persistence-of-Vision Motion. In *Proceedings of the 2026 CHI Conference on Human Factors in Computing Systems (CHI '26)*. Association for Computing Machinery, New York, NY, USA, Article 749, 19 pages. doi:10.1145/3772318.3790357
Tomohiro Yendo, Toshiaki Fujii, Masayuki Tanimoto, and Mehrdad Panahpour Tehrani. 2010. The Seelinder: Cylindrical 3D display viewable from 360 degrees. *Journal of Visual Communication and Image Representation* 21, 5-6 (July 2010), 586–594. doi:10.1016/j.jvcir.2009.10.004
Tomohiro Yendo, Naoki Kawakami, and Susumu Tachi. 2005. Seelinder: the cylindrical lightfield display. In *ACM SIGGRAPH 2005 Emerging technologies on - SIGGRAPH '05*. ACM Press, Los Angeles, California, 16. doi:10.1145/1187297.1187314
Darryl Yong. 2006. Strings, Chains, and Ropes. *SIAM Rev.* 48, 4 (Jan. 2006), 771–781. doi:10.1137/050641910
Shunsuke Yoshida. 2016. fVisiOn: 360-degree viewable glasses-free tabletop 3D display composed of conical screen and modular projector arrays. *Optics Express* 24, 12 (June 2016), 13194. doi:10.1364/OE.24.013194

A Additional figures

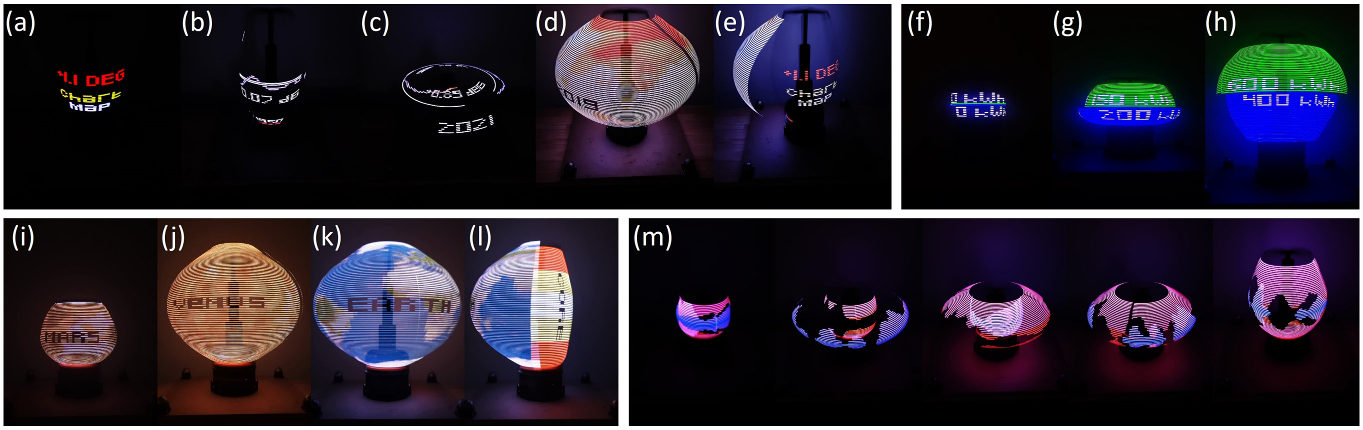

Fig. 6. Applications of the MorphSkein system. **(top left)** The system *adapts its axisymmetric display shape to context*. In this interactive museum exhibit on climate change, it morphs into a cylinder-like display to present (a) rotating textual summaries of global temperature rise since 1880 or (b) a rotating line chart of year-by-year temperature changes to surrounding visitors. It then (c) transitions to a disk-like configuration, transforming the linear chart into a circular overview of the full temporal dataset. When geographical context is needed, the system further (d) morphs into a sphere-like display to render a global temperature heatmap on a planet-shaped surface. Portions of the sphere can be selectively removed to return to a cylinder-like form, enabling a switch back to textual or line-chart visualizations for specific nearby visitors. (**top right**) The system *encodes 360°-visible data*. In public spaces, workspaces or households, it shows cumulative energy production (green) and consumption (blue) over (f) 0, (g) 15, and (h) 30 days, supporting shared awareness of energy information from any viewing angle. (**bottom left**) The system *renders axisymmetric 3D objects*. In museums, classrooms, or planetariums, it displays planetary surfaces—(i) Mars, (j) Venus, (k) Earth—and (l) their internal layers, preserving proportions for fair comparison of size, structure, and appearance. (**bottom right**) The system *augments traditional visualizations* with omnidirectional, mesmerizing transformations. In music festivals, art galeries or performance spaces, it (m) renders dynamic audio spectrum analyzers that surround the display, creating an immersive visual experience that entertains attendees from all directions.

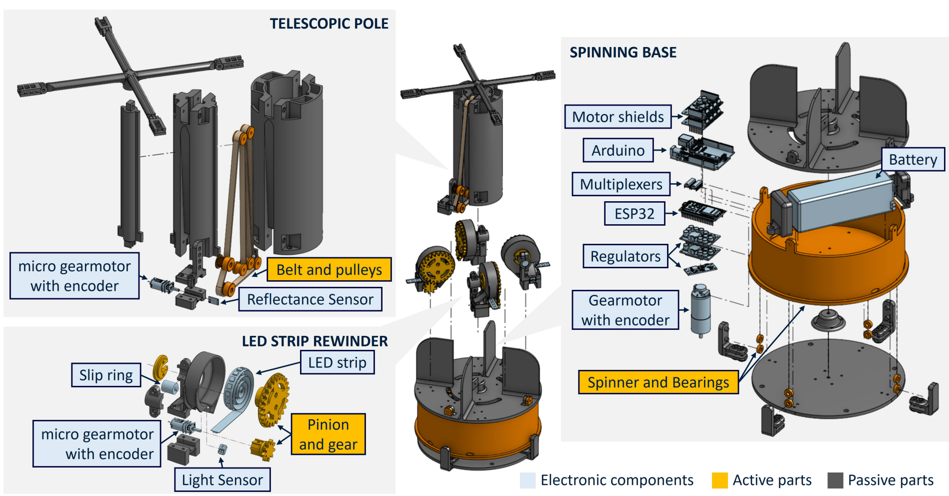

Fig. 7. Exploded view of the MorphSkein system. All parts are 3D printed. (**top left**) The *telescopic pole* consists of three concentric stages, each with pulleys at both ends. They are connected by a GT2 belt driven by a Polulu micro gearmotor (12V, 380:1) and a magnetic encoder (2.7-18V, 12 CPR). To reset, the motor retracts the stages until a Polulu QTR-1A sensor detects a reflective tape on the belt, marking the 200mm reset position. (**bottom left**) Each of the four *LED strip rewinders* houses a 1-meter Adafruit DotStar LED strip (5V, 144 LEDs) rolled within a gear wheel and soldered to a miniature slip ring (6 wires, 240V @ 2A). At the exit, a Polulu micro gearmotor (12V, 380:1) with a magnetic encoder and an Adafruit ALS-PT19 light sensor control rewinding; to reset, the pole retracts to 200mm, all LEDs except the 31st are turned off and lit red, and the motor rewinds until the light sensor detects the red light, ensuring a minimum length of 217mm (31 LEDs). (**right**) At the center of the *spinning base*, is mounted a Polulu Metal Gearmotor (12V, 9.7:1, 25Dx63L mm) with a Magnetic Encoder (12V, 48 CPR). The base houses the electronics, including a power supply. An Arduino Uno Wifi Rev2 with two Motoron M3S256 Motor Shields drives the motors and reads sensors, while an ESP32 DevKit V1 with two 74HC4051 multiplexers controls the LED strips via SPI. Communication between the ESP32 and Arduino is via serial connection. Power is supplied by a Zeee 11.1V 8000mAh 3S Lipo Battery, with two Pololu 5V@15A regulators powering the boards, sensors, and LED strips, and a Pololu 12V@7A Step-Up Voltage Regulator powering the shields and motors. A ground station (desktop computer) uses WiFi and WebSocket to remotely control the system, exchange target and measured values of (v, h, l), and stream video frames $I : (x, y) \mapsto (r, g, b)$ via a Node-RED dashboard.

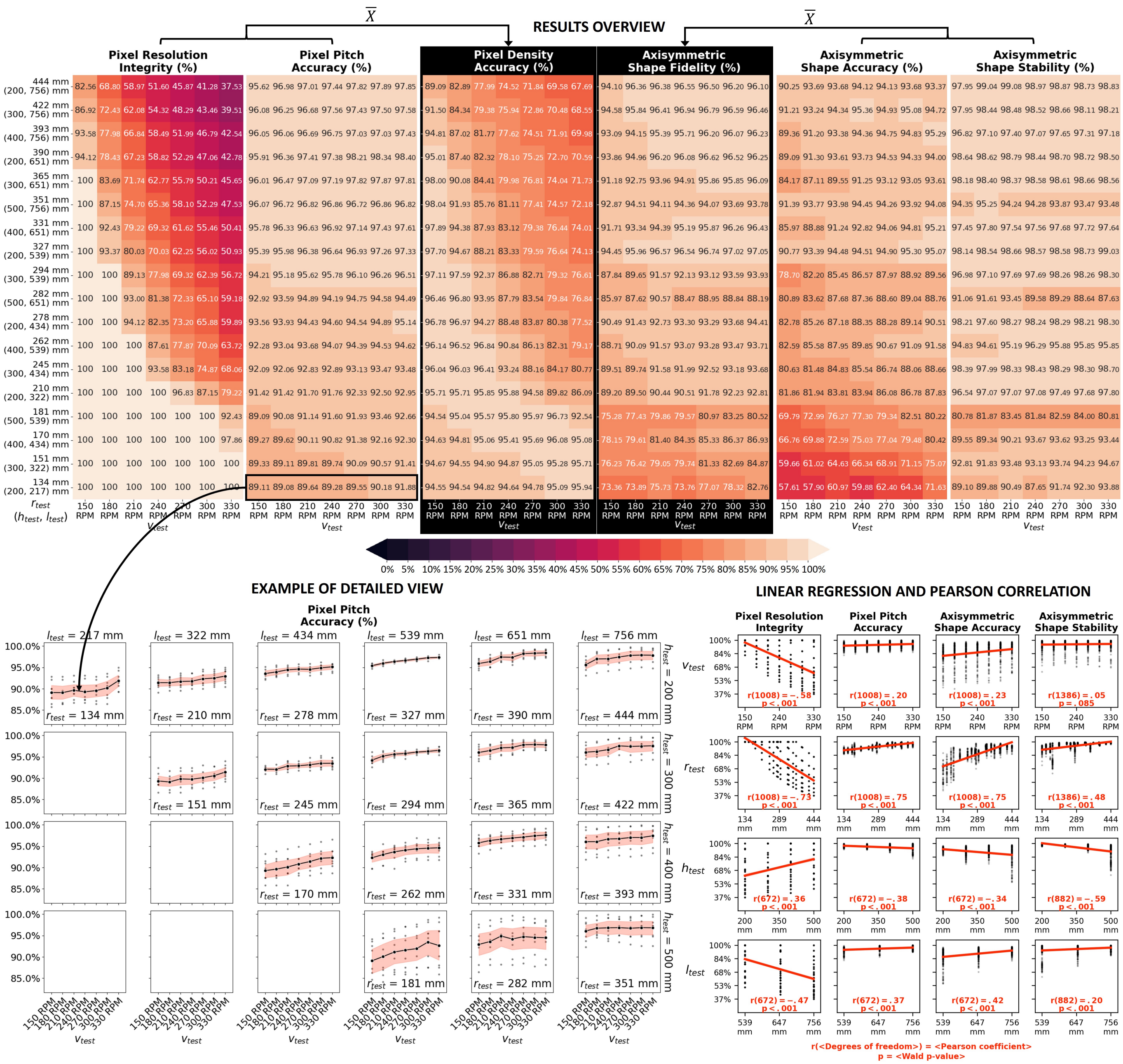

Fig. 8. (**top**) Overview heatmap showing the mean value of each response variable across trials for all pole height (h_{test}) and strip length (l_{test}) configurations, plotted as a function of angular speed (v_{test}). Configurations are ordered by increasing resulting display radius (r_{test}). (**bottom left**) Detailed facet-grid example for pixel pitch accuracy. Each panel corresponds to a (h_{test}, l_{test}) configuration and shows individual trial measurements with the mean and 95% confidence interval as a function of angular speed (v_{test}). The panel means correspond to the values shown in the overview heatmap. (**bottom right**) Facet grid of individual trial data with linear regression fits for each factor–response variable pair. Panels are annotated with the Pearson correlation coefficient and Wald p-value.